
MeshSplats: Mesh-Based Rendering with Gaussian Splatting Initialization

Rafał Tobiasz^{*1} Grzegorz Wilczyński^{*1} Marcin Mazur¹ Sławomir Tadeja² Przemysław Spurek¹

Abstract

Gaussian Splatting (GS) is a recent and pivotal technique in 3D computer graphics. GS-based algorithms almost always bypass classical methods such as ray tracing, which offers numerous inherent advantages for rendering. For example, ray tracing is able to handle incoherent rays for advanced lighting effects, including shadows and reflections. To address this limitation, we introduce MeshSplats, a method which converts GS to a mesh-like format. Following the completion of training, MeshSplats transforms Gaussian elements into mesh faces, enabling rendering using ray tracing methods with all their associated benefits. Our model can be utilized immediately following transformation, yielding a mesh of slightly reduced quality without additional training. Furthermore, we can enhance the reconstruction quality through the application of a dedicated optimization algorithm that operates on mesh faces rather than Gaussian components. The efficacy of our method is substantiated by experimental results, underscoring its extensive applications in computer graphics and image processing. The source code is available at <https://github.com/gwilczyński95/meshsplats>.

1. Introduction

In the domain of computer graphics, the efficient representation of 3D objects is of paramount importance. Classical techniques employ meshes for convenient storage and rapid rendering (Foley et al., 1994). Moreover, different ray tracing methods that can be performed on top of such mesh representations enable various advantages, such as handling incoherent rays for secondary lighting effects, including shadows and reflections (Peddie, 2019).

Unfortunately, training mesh-like representations directly on 2D images presents significant challenges. Gaussian

Splatting (GS) framework (Kerbl et al., 2023) addresses this problem by representing a 3D scene as a set of Gaussian distributions characterized by parameters such as mean, covariance, opacity, and color, often expressed in terms of spherical harmonics. This representation can be effectively trained to achieve high-quality reconstructions and real-time rendering. However, we should note that GS is, in essence, a rasterization technique that utilizes Gaussian projections instead of ray tracing. This inherent characteristic of GS presents a challenge when attempting to incorporate lighting, shadow, or reflection effects (Kerbl et al., 2023; Moenne-Loccoz et al., 2024), as it is not a straightforward process due to key differences between rasterization and ray tracing. Typically, the former has been employed to achieve real-time performance by approximating the formation of images. In contrast, ray tracing has enabled comprehensive, high-quality rendering but usually works with mesh-based representations.

A potential approach to address this limitation is integrating GS training with ray tracing, a technique referred to as 3D Gaussian Ray Tracing (3DGRT) (Moenne-Loccoz et al., 2024). This method has yielded excellent visual effects, incorporating light reflection and shadows. Additionally, it enables the integration of 3D scenes with mesh-based models. 3DGRT employs bounding primitives that encompass each Gaussian and facilitate the efficient application of the ray tracing model on these primitives instead of directly on the Gaussians. In RaySplat (Byrski et al., 2025), the authors use ellipses as an approximation of Gaussians instead of bounding primitives. The above methods use ray tracing approaches for rendering and can model light effects but require dedicated rendering environments. LinPrim (von Lützwow & Nießner, 2025) employs linear primitives such as octahedra and tetrahedra for differentiable volumetric rendering. This method utilizes mesh-based primitives instead of Gaussians. The model is capable of producing renders of superior quality. However, it necessitates a specialized environment for both training and rendering.

To solve these problems, we propose MeshSplats, a method that directly converts Gaussian components into mesh-like representations that can be rendered in existing rendering

^{*}Equal contribution ¹Jagiellonian University ²University of Cambridge. Correspondence to: Przemysław Spurek <przemyslaw.spurek@uj.edu.pl>.

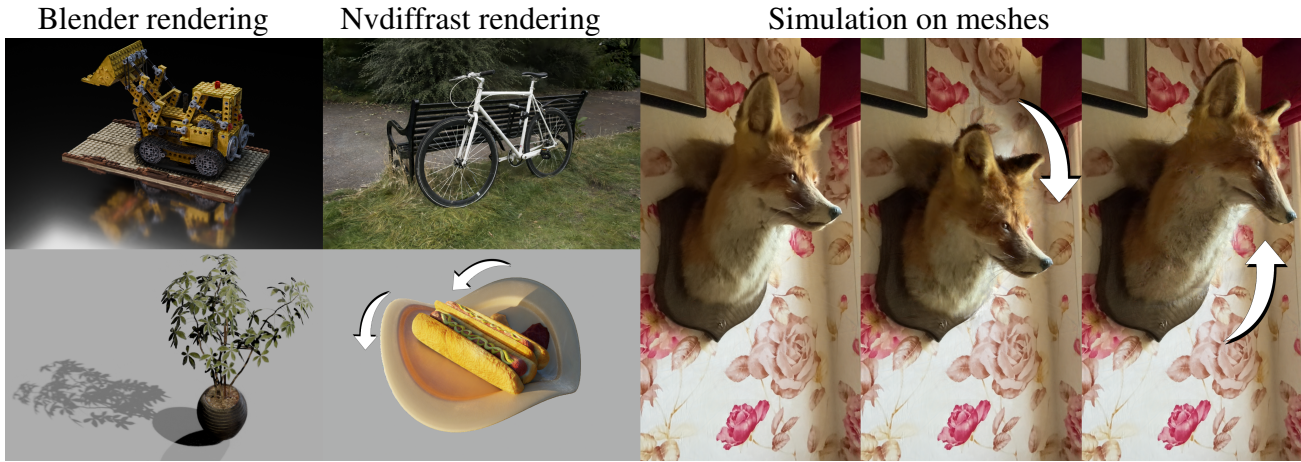


Figure 1. MeshSplats (our) facilitates the conversion of Gaussian Splatting into a mesh format, which can subsequently be rendered using prevailing tools such as Blender and Nvdiffrast. This transformation enables sophisticated lighting effects, including reflections and shadows, as well as the capacity to execute mesh-based simulations.

environments such as Blender¹ or Nvdiffrast² (Munkberg et al., 2022) (see Fig. 1). Specifically, we first obtain a set of disjoint meshes (see Fig. 2) with colors and opacities. Next, we use ray tracing to render objects with lightning effects on this mesh-based representation. In such a procedure, the main component of the vanilla GS is the opacity of particles. To this end, we employ Nvdiffrast, a PyTorch library that facilitates high-performance primitive operations for rasterization-based differentiable rendering. We utilize this method as it enables efficient rendering of meshes derived from GS. However, it is noteworthy that alternative renderers, such as Blender, can also be used, though the quality of the outputs is constrained due to the significance of transparency in GS techniques (see Fig. 1).

MeshSplats technique is dedicated to flat Gaussians, which possess a single scaling parameter. These Gaussians are capable of undergoing effective training and can attain comparable rendering quality. Furthermore, flat Gaussians exhibit a comparable morphology to meshes. Consequently, their conversion into mesh faces is more straightforward than that of classical 3D Gaussians. Therefore, while the use of flat Gaussians may result in a certain compromise in efficiency, their application with MeshSplats is well-feasible.

Moreover, transformation proposed by our method converts GS into a mesh to facilitate direct rendering. Therefore, to produce high-quality reconstructions, we can use a GS-based approach with meshes instead of classical Gaussians to improve quality. This enables the integration of our method with lighting and shadow effects (see Fig. 3).

¹<https://www.blender.org>

²<https://nvlabs.github.io/nvdiffrast>

In summary, our work contributes the following:

- we introduce MeshSplats, a novel method that facilitates the conversion of GS with flat Gaussians into mesh-based representation, allowing further integration of dedicated tools;
- MeshSplats uses ray tracing, which allows for the processing of incoherent rays for secondary lighting effects such as shadows and reflections rendered from highly distorted cameras;
- MeshSplats is capable of being rendered in traditional rendering environments, thus obviating the necessity of employing specialized GS renderers;
- our quantitative and qualitative experimental results confirm that MeshSplats attains rendering quality comparable to Gaussian Splatting while enabling the benefits of mesh-based representations;
- we show that MeshSplats optimization pipeline effectively reduces artifacts and refines fine geometric details, leading to enhanced geometric accuracy and photorealistic rendering.

2. Related Work

Our work establishes a connection between advancements in GS and classical ray tracing-based rendering while concurrently addressing the limitations of rasterization-centric approaches. Here, we review the relevant literature across four primary areas.

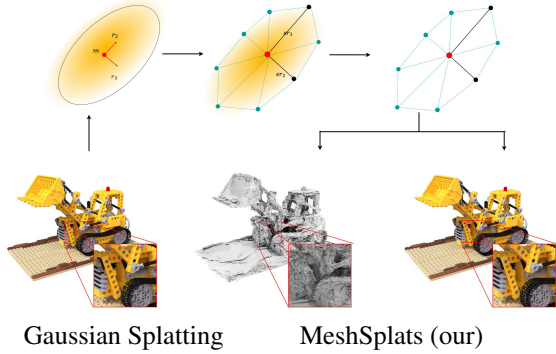


Figure 2. Transformation of a flat Gaussian into a mesh by MeshSplats (our), where m is the mean of the Gaussian, r_2 and r_3 are the second and third columns of the rotation matrix R (see Eq. (1)), while sr_1 and sr_2 denote scaled_rot₁ and scaled_rot₂ from Eq. (3).

Neural Radiance Fields and View-Dependent Effects

Neural Radiance Fields (NeRFs) (Mildenhall et al., 2021) revolutionized novel view synthesis by modeling scenes as implicit neural representations. Subsequent works improved rendering quality (Barron et al., 2021; 2022; 2023) and efficiency (Chen et al., 2022; Fridovich-Keil et al., 2022; Müller et al., 2022), while methods such as Ref-NeRF (Verbin et al., 2022) and SpecNeRF (Ma et al., 2024) enhanced view-dependent effects using reflected directions and Gaussian encoding. NeRF-Casting (Verbin et al., 2024) introduced ray marching along reflection paths for realistic near-field illumination, but such approaches remain computationally intensive and unsuitable for real-time applications. In contrast, GS-based methods achieve real-time rendering but lack nuanced handling of reflections and shadows.

Gaussian Splatting and Rendering Limitations

3D Gaussian Splatting (3DGS) (Kerbl et al., 2023) was a breakthrough, representing scenes as anisotropic Gaussians optimized by differentiable rasterization. Extensions such as Mip-Splatting (Yu et al., 2024) reduced aliasing, while 2DGS (Huang et al., 2024) improved surface alignment by restricting the Gaussians to 2D manifolds. However, these methods rely on spherical harmonics (SH) to approximate view-dependent effects, leading to blurry reflections under complex lighting. Recent work such as GaussianShader (Jiang et al., 2024) and 3DGS-DR (Ye et al., 2024) incorporated environment maps for reflections but were limited to distant lighting. 3iGS (Tang & Cham, 2025) introduced illumination fields via tensorial factorization, but bounded scene assumptions limit real-world applicability. Crucially, all these methods rely on rasterization, which struggles with the incoherent rays required for advanced effects like shadows and inter-reflections.

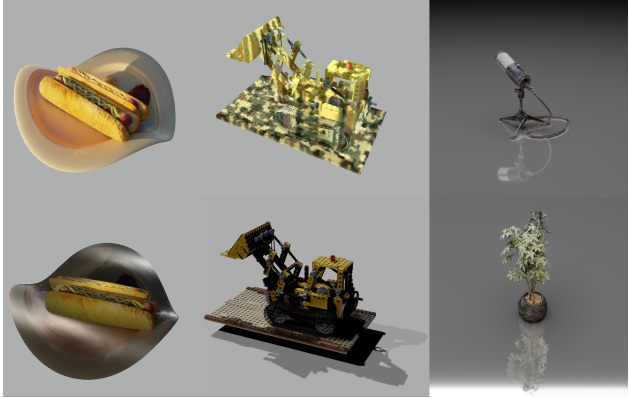


Figure 3. Examples of renderings produced by MeshSplats (our), with lighting conditions and mesh deformations applied using Blender or Nvdiffrast. The rendered objects exhibit various lighting effects, with the top-middle render showcasing an object with a blended texture. The underlying original images (not shown here) were taken from the NeRF Synthetic dataset.

Ray Tracing with Gaussian Representations

Recent efforts integrate ray tracing with GS to overcome rasterization limitations. 3D Gaussian Ray Tracing (3DGRT) (Moenne-Loccoz et al., 2024) uses bounding primitives around Gaussians, enabling GPU-accelerated ray tracing via NVIDIA OptiX (Parker et al., 2010). While efficient, 3DGRT approximates Gaussians as polytopes, making compatibility with flat Gaussians (Huang et al., 2024) and non-Gaussian distributions difficult. EnvGS (Xie et al., 2024) introduces environment Gaussians to model reflections but remains limited to GS-specific rendering pipelines. Similarly, IRGS (Gu et al., 2024) proposes differentiable 2D Gaussian ray tracing for inverse rendering but requires complex Monte Carlo sampling. These methods highlight the potential of ray tracing and simultaneously inherit the structural limitations of GS, such as dependence on custom renderers and approximations that hinder generalization.

Mesh-Based Rendering and Hybrid Approaches

Classical mesh representations facilitate efficient ray tracing. However, they are challenging to optimize directly from images. Our work addresses this gap by converting GS to mesh-like structures, leveraging the optimization strengths of GS while maintaining compatibility with traditional renderers such as Blender and Nvdiffrast (Munkberg et al., 2022). In contrast to the polytope approximations (Moenne-Loccoz et al., 2024), our method preserves geometric fidelity by mapping flat Gaussians to mesh faces, thereby avoiding artifacts from bounding primitives. This approach is analogous to mesh splatting techniques (Weyrich et al., 2007), yet it emphasizes post-training conversion rather than direct mesh optimization.

3. MeshSplats Transformation

The core of our approach consists of three straightforward steps. First, we use classical GS to create a collection of Gaussians. Next, we apply MeshSplats to transform the Gaussian element into separate mesh faces that approximate the shape of the Gaussians while preserving color and opacity. This step results in a high-quality reconstruction, although minor artifacts may still be visible. Finally, we refine this representation similarly to GS, using separate mesh faces instead of Gaussians. The scheme of the MeshSplats transformation is shown in Fig. 2.

In the following, we provide a detailed description of our approach. We start with a recall of the conventional GS technique. Next, we introduce the parametrization of MeshSplats. Our model is designed to work with general Gaussian distributions, emphasizing its suitability for flat Gaussians. Thus, we will focus on flat Gaussians and then move on to 3D Gaussians. We then illustrate how MeshSplats can be integrated with traditional mesh rendering tools, with the best results achieved using Nvdiffrast rendered (Munkberg et al., 2022), as it efficiently handles multiple components with different opacities. Finally, we show that MeshSplats can be fine-tuned similarly to GS.

Gaussian Splatting The GS technique is employed to construct a 3D scene through the utilization of a set of 3D Gaussians:

$$(\mathcal{N}(\mathbf{m}, \Sigma), \sigma, c),$$

with the definition of each element being contingent upon its position (mean) \mathbf{m} , the corresponding covariance matrix Σ , the opacity σ , and the color c . The representation of color employs the Spherical Harmonics (SH) approach (Fridovich-Keil et al., 2022; Müller et al., 2022). However, it is pertinent to note that the alternative of substituting SH with conventional RGB colors is permissible, albeit resulting in a marginal decline in reconstruction quality, primarily owing to its insensitivity to the viewing direction. In MeshSplats, we employ a conventional renderer for meshes, necessitating the use of RGB colors. This approach yields a marginally diminished rendering quality compared to traditional GS, yet it facilitates the incorporation of external lighting.

The GS algorithm constructs the NeRF representation through sequential optimization of the 3D Gaussian parameters. This technique is efficient due to its rendering process, which relies on projecting Gaussian components. The GS optimization method involves iteratively rendering and comparing the resulting images to the input views from the dataset. However, projecting from 3D to 2D can result in a misplacement of geometry. Therefore, the GS optimization must adjust the scene by creating, removing, or repositioning geometry as needed. Accurate 3D Gaussian covariances

are paramount for a concise representation, as expansive uniform regions can be efficiently covered using fewer large anisotropic Gaussians.

MeshSplats Transformation for Flat Gaussians As mentioned above, in the classical GS model, each element is characterized by a collection of parameters, including a covariance matrix Σ , which is factorized as

$$\Sigma = RSSR^T, \quad (1)$$

where R is the rotation matrix, and S is a diagonal matrix containing the scaling parameters. There are few approaches that use flat Gaussians (Guédon & Lepetit, 2024; Waczyńska et al., 2024; Huang et al., 2024), but we use the GaMeS representation (Waczyńska et al., 2024), given as:

$$\mathcal{N}(\mathbf{m}, R, S), \quad (2)$$

where \mathbf{m} is the mean of the Gaussian, $S = \text{diag}(s_1, s_2, s_3)$, with $s_1 = \epsilon$, and R is the rotation matrix defined as $R = [\mathbf{r}_1, \mathbf{r}_2, \mathbf{r}_3]$, with $\mathbf{r}_i \in \mathbb{R}^3$. Thus, Gaussian components can be approximated by mesh faces. Our model uses a simple mesh constructed from a polygon inscribed in an ellipse, as shown in Fig. 2.

The transformation of flat Gaussians into meshes is achieved through a series of steps controlled by three hyperparameters: a scale multiplier *scale_mul*, a number of triangles per Gaussian *no.triag*, and an opacity multiplier *opac.mul*. Each Gaussian is represented as a mesh centered at its mean position, with its shape and orientation determined by its scale and rotation parameters. Given that the Gaussians are treated as 2D structures, the scale ($s_i = \epsilon$, where s_i is negligible) and its corresponding rotation vector are discarded, effectively reducing the problem to two dimensions.

First, two orthogonal vectors defining the major and minor axes of an ellipse are computed as follows:

$$\begin{aligned} \text{scaled_rot}_1 &= \text{scale_mul} \cdot \exp(s_2) \cdot \mathbf{r}_2, \\ \text{scaled_rot}_2 &= \text{scale_mul} \cdot \exp(s_3) \cdot \mathbf{r}_3, \end{aligned} \quad (3)$$

where \mathbf{r}_2 and \mathbf{r}_3 are the second and third columns, respectively, of the rotation matrix R , and $\text{scale_mul} = 2.7$. Next, *no.triag* points are generated at the boundary of the ellipse and used to construct the mesh. This is done by calculating *no.triag* evenly distributed angles θ_i in the range $[-\pi, \pi]$. For each angle θ_i , the vertex \mathbf{v}_i is computed as follows:

$$\mathbf{v}_i = \mathbf{m} + \cos(\theta_i) \cdot \text{scaled_rot}_1 + \sin(\theta_i) \cdot \text{scaled_rot}_2. \quad (4)$$

The mesh is then constructed as a triangle fan, where all triangles share a common origin point at the ellipse’s center. Each triangular face is defined by the center point and two consecutive boundary vertices, resulting in *no.triag* triangles per Gaussian. This structure approximates the flat

Gaussian as a set of connected triangles. In all experiments, we used $no_triag = 8$.

In our method, color is assigned to each vertex in the mesh, and all vertices inherit the color of the corresponding Gaussian. This ensures that the mesh visually represents the Gaussian’s color in the final rendering. Gaussians are trained without Spherical Harmonics, guaranteeing compatibility with mesh renderers. On the other hand, opacity is assigned to each vertex in the mesh, with all vertices inheriting the color of the corresponding Gaussian. For the boundary vertices, the opacity is scaled by $opac_mul$ to create a linear interpolation of the opacity across the mesh. This approximates the decrease in Gaussian opacity, with the rate controlled by the $opac_mul$ parameter. In all experiments, $opac_mul = 0.2$.

Notably, through this process, each flat Gaussian is transformed into a mesh that preserves its spatial extent, orientation, and visual properties. The hyperparameters $scale_mul$, no_triag , and $opac_mul$ provide control over the fidelity and appearance of the resulting triangle soup, thereby enabling a flexible and accurate representation of spatial Gaussians.

MeshSplats Transformation for 3D Gaussians The transformation of 3D Gaussians into meshes builds upon the methodology used for flat Gaussians, but extends it to three dimensions. While the 2D approach approximates Gaussians as flat ellipses, the 3D approach represents them as ellipsoids, capturing their full spatial extent. The process is governed by three hyperparameters, $scale_mul$, no_triag , and $opac_mul$, which maintain the same values as in the 2D case. However, it should be noted that several significant distinctions emerge due to the augmented dimensionality. Thus, unlike the 2D case where the smallest scale and its corresponding rotation vector are discarded, all three scale constants and rotation vectors are retained for 3D Gaussians. A graphical summary of the transformation process is shown in Fig. 4.

First, three orthogonal vectors defining the principal axes of an ellipsoid are computed as follows:

$$\begin{aligned} scaled_rot_1 &= scale_mul \cdot \exp(s_1) \cdot \mathbf{r}_1, \\ scaled_rot_2 &= scale_mul \cdot \exp(s_2) \cdot \mathbf{r}_2, \\ scaled_rot_3 &= scale_mul \cdot \exp(s_3) \cdot \mathbf{r}_3, \end{aligned} \quad (5)$$

where \mathbf{r}_1 , \mathbf{r}_2 , and \mathbf{r}_3 are respective columns of the rotation matrix R . These vectors define the orientation and extent of the ellipsoid in 3D space. Next, no_triag points are generated at the boundary of each of the three orthogonal surfaces defined by the pairs $(scaled_rot_1, scaled_rot_2)$, $(scaled_rot_1, scaled_rot_3)$, and $(scaled_rot_2, scaled_rot_3)$. For each surface, no_triag uniformly distributed angles θ_i in the range $[-\pi, \pi]$ are com-

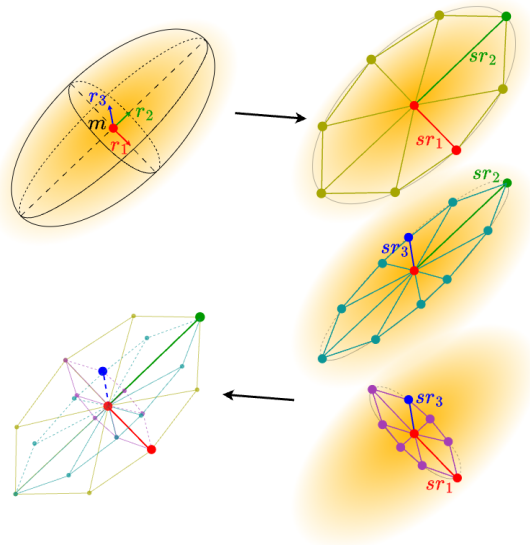


Figure 4. Transformation of a 3D Gaussian into a mesh by MeshSplats (our). Here m is the mean of the Gaussian, r_1 , r_2 , and r_3 are columns of the rotation matrix R , and sr_1 , sr_2 , and sr_3 represent $scaled_rot_1$, $scaled_rot_2$, and $scaled_rot_3$ from Eq. (5). The transformation is performed analogously to the flat case (see Fig. 2), but it is extended to the three surfaces spanned by the vector pairs (r_1, r_2) , (r_1, r_3) , and (r_2, r_3) . Meshes are created for each surface and combined into a single mesh representing the 3D Gaussian.

puted. Then, for every angle θ_i , the vertex v_i is calculated in a similar way as for the 2D method, i.e.:

$$v_i = \mathbf{m} + \cos(\theta_i) \cdot scaled_rot_a + \sin(\theta_i) \cdot scaled_rot_b, \quad (6)$$

where $scaled_rot_a$ and $scaled_rot_b$ are vectors that span the current surface. Points at surface intersections are shared to avoid redundant vertices and ensure a seamless mesh structure.

The mesh is then constructed as a collection of triangle fans, assigning one fan to each surface. Each triangular face is defined analogously to the 2D method, resulting in $3 \cdot no_triag$ triangles per Gaussian. This structure approximates the 3D Gaussian as a set of connected triangles distributed across three orthogonal surfaces. Color and opacity are assigned to each vertex in the mesh in the same manner as in the 2D solution.

Note that this process transforms each 3D Gaussian into a mesh in much the same way as in the previous case. The main difference is the use of three orthogonal faces to capture the entire 3D structure, as well as the sharing of vertices between faces to maintain mesh efficiency. However, this representation has more vertices and triangles than the 2D case, resulting in a model with higher memory usage and slower rendering.

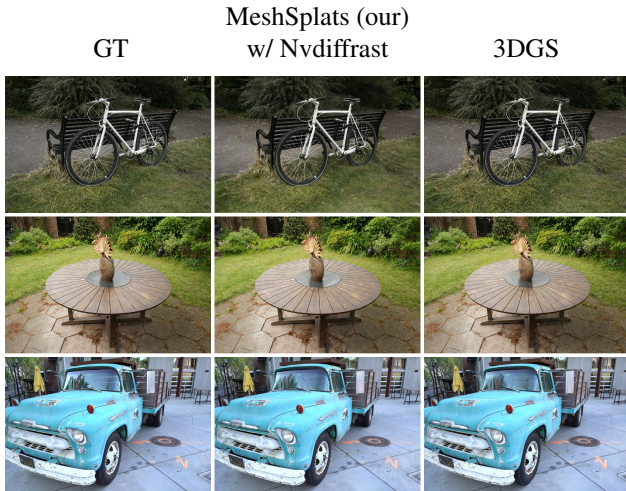


Figure 5. Examples of renderings of different types: the first column shows the ground truth image, the second column shows the rendering of the optimized MeshSplats (our) using Nvdiffrast, and the third column shows the rendering of 3D Gaussian Splatting with spherical harmonics set to zero. The first two rows comprise data from the Mip-NeRF360 dataset, where both MeshSplats and 3DGS were optimized with the resolution parameter set to 4. The last row is composed of the Truck example from the Tanks and Templates dataset, where both MeshSplat and 3DGS were optimized with the resolution parameter set to one.

Rendering MeshSplats in Nvdiffrast The rasterization process, facilitated by Nvdiffrast on a mesh soup, involves the transformation of 3D vertices into 2D screen space, culminating in rendering these vertices as an image. The process initiates with transforming vertices into clip space utilizing a model-view-projection (MVP) matrix, which maps them into normalized device coordinates. This step ensures that the vertices are appropriately positioned for rendering on the screen.

The rasterization process utilizes a depth-peeling technique to manage transparency and overlapping geometry. This method involves the iterative rendering of the scene in multiple layers, ensuring that each layer is correctly composited with the others. The rasterized output and its derivatives are computed for each layer, enabling precise interpolation of vertex colors across the triangles. The interpolated colors are then blended with the accumulated colors from previous layers, taking into account transparency through the alpha channel. This blending process ensures that transparent regions are accurately represented in the final image.

Once all layers have been processed, the final RGB and alpha values are extracted from the accumulated color buffer. The RGB values represent the rendered image, while the alpha channel captures the transparency. This approach takes advantage of Nvdiffrast’s efficiency and flexibility to



Figure 6. Examples of renderings of different types: the first column shows the ground truth image, the second column shows the rendering of the optimized MeshSplats (our) using Blender with the EEVEE renderer, where the material is configured with the HASHED blend method and backface culling is disabled, and the third column shows the rendering of 3D Gaussian Splatting with spherical harmonics set to zero. All images were taken from the NeRF Synthetic dataset. Differences in colors between ground truth and Blender renders are caused by different lightning conditions.

render complex objects, making it particularly suitable for scenes with detailed geometry and transparency. Depth peeling ensures that overlapping elements are handled correctly, producing high-quality renderings.

Finetuning of MeshSplats Our fine-tuning pipeline accepts the mesh soup created from the Gaussians (either 2D or 3D) as input and refines it to match the target scene better. The pipeline consists of several stages, including transformation, rasterization, blending, and loss computation, followed by iterative optimization and pruning. In the subsequent description, we provide a thorough overview of each step in the pipeline.

Transformation of Vertices. As previously mentioned, the input mesh soup vertices are transformed using the MVP matrix. This matrix projects the 3D vertices into the 2D image space for rasterization. Each vertex v_i is then transformed as follows:

Table 1. Quantitative evaluation of MeshSplats (our) on the Mip-NeRF360 (Barron et al., 2022), Tanks and Temples (Knapitsch et al., 2017), and Deep Blending (Hedman et al., 2018) datasets. We provide a comparison to the following state-of-the-art baselines: Plenoxels (Fridovich-Keil et al., 2022), INGP (Müller et al., 2022), M-NeRF360 (Barron et al., 2021), 3DGS (Kerbl et al., 2023), 3DGRT (Moenne-Loccoz et al., 2024), LinPrim (von Lützwow & Nießner, 2025), RadiantFoam (Govindarajan et al., 2025), and RaySplats (Byrski et al., 2025). On Mip-NeRF360 and Tanks and Temples, MeshSplats achieves comparable results to rasterization-based techniques despite its mesh-based representation. In addition, MeshSplats shows superior performance on Deep Blending, proving its effectiveness for indoor geometries. Note that LinPrim lacks results on the Tanks and Temples and Deep Blending datasets (see (von Lützwow & Nießner, 2025)), while RadiantFoam only lacks results on the latter (see (Govindarajan et al., 2025)).

		Mip-NeRF360			Tanks and Temples			Deep Blending		
		SSIM \uparrow	PSNR \uparrow	LPIPS \downarrow	SSIM \uparrow	PSNR \uparrow	LPIPS \downarrow	SSIM \uparrow	PSNR \uparrow	LPIPS \downarrow
Spherical Harmonics	Plenoxels	0.670	23.63	0.44	0.379	21.08	0.795	0.510	23.06	0.510
	INGP-Base	0.725	26.43	-	0.723	21.72	0.330	0.797	23.62	0.423
	INGP-Big	0.751	26.75	0.30	0.745	21.92	0.305	0.817	24.96	0.390
	M-NeRF360	0.844	29.23	-	0.759	22.22	0.257	0.901	29.40	0.245
	3DGS-30K	0.87	28.69	0.22	0.841	23.14	0.183	0.903	29.41	0.243
	3DGRT	0.854	28.71	0.25	0.830	23.20	0.222	0.900	29.23	0.315
	LinPrim	0.803	26.63	0.221	-	-	-	-	-	-
	RadiantFoam	0.83	28.47	0.21	-	-	-	0.89	28.95	0.26
RGB	RaySplats	0.846	27.31	0.237	0.829	22.20	0.202	0.900	29.57	0.320
	MeshSplats (our)	0.817	28.08	0.229	0.766	21.71	0.248	0.890	29.50	0.254

$$\mathbf{v}_i^{\text{transformed}} = \text{MVP} \cdot \mathbf{v}_i. \quad (7)$$

Rasterization and Blending. The rasterization and blending processes adhere to the methodology above, employing depth peeling to manage overlapping meshes with varying opacities. The output image is derived by integrating multiple rasterized layers, thereby ensuring the preservation of each mesh element’s contribution.

Loss Function. The loss function employed for optimization constitutes a weighted combination of L_1 loss and the structural similarity index measure (SSIM). This approach is analogous to that utilized in 3D Gaussian Splatting. Consequently, the loss is defined as follows:

$$\mathcal{L} = \lambda \cdot L_1(\hat{y}, y) + (1 - \lambda) \cdot \text{SSIM}(\hat{y}, y), \quad (8)$$

where y is the ground truth image, \hat{y} is the predicted image, and $\lambda = 0.6$ is a balancing constant.

Optimization and Pruning. The optimization process updates the mesh soup vertices to minimize the loss function given in Eq. (8). Specifically, the colors and opacities of the vertices are optimized with a learning rate lr_{color} . The positions of the vertices are also optimized, but with a weaker learning rate of $lr_{\text{verts}} = \exp(-3) \cdot lr_{\text{color}}$, to ensure that the position updates are subtle and stable.

Every 10 epochs, a pruning step is performed to remove redundant faces and vertices. A face is pruned if all its vertices have an opacity below a $\exp(-4)$ threshold. Additionally, if any other face does not use the vertices of the

pruned face, they are also deleted. This pruning step helps reduce memory usage and computational complexity while maintaining the fidelity of the scene representation.

4. Experiments

In this section, we present the outcomes of our experimental study, encompassing both quantitative and qualitative results. To elucidate the functionality of MeshSplats with varying GS initializations, we have conducted a respective ablation study. Furthermore, we elucidate the behavior of our algorithm subsequent to parametrization and training. The source code, together with additional experimental results, is available at <https://github.com/gwilczynski95/meshsplats>.

Datasets and Metrics The proposed MeshSplats framework was evaluated across three standard datasets: MipNeRF360 (Barron et al., 2022), Tanks and Temples (Knapitsch et al., 2017), and Deep Blending (Hedman et al., 2018). To ensure consistency, the same scenes as in (Moenne-Loccoz et al., 2024) were examined. Specifically, for Mip-NeRF360, we conducted an analysis of four indoor scenes (room, counter, kitchen, and bonsai) and three outdoor scenes (bicycle, garden, and stump). For the Tanks and Temples dataset, our focus was on two extensive outdoor scenes (train and truck). Additionally, for the Deep Blending dataset, we included two indoor scenes (playroom and drjohnson). In accordance with prior works, images for evaluation are downsampled by a factor of two for indoor and four for outdoor scenes. All datasets share uniform train/test splits.

Table 2. The results of the ablation study examining the impact of different GS initialization techniques on the performance of MeshSplats (our). Since our model is dedicated to flat Gaussians, it generally provides better results when initialized with 2DGS (Huang et al., 2024) or GaMeS (Waczyńska et al., 2024). Nevertheless, we emphasize that in the case of the classic 3DGS (Kerbl et al., 2023), MeshSplats achieves comparable performance to other methods on both the Mip-NeRF360 and Tanks and Templates datasets. In addition, for the Deep Blending dataset, MeshSplats (when initialized with 2DGS) achieved superior PSNR compared to 3DGS, GaMeS, and 2DGS.

	Mip-NeRF360			Tanks and Temples			Deep Blending		
	SSIM ↑	PSNR ↑	LPIPS ↓	SSIM ↑	PSNR ↑	LPIPS ↓	SSIM ↑	PSNR ↑	LPIPS ↓
3DGS RGB	0.873	28.63	0.141	0.837	23.02	0.190	0.899	29.27	0.249
3DGS MeshSplats (our)	0.809	27.95	0.234	0.729	21.35	0.310	0.876	28.68	0.260
GaMeS RGB	0.871	28.62	0.144	0.834	23.05	0.193	0.897	29.23	0.252
GaMeS MeshSplats (our)	0.818	28.08	0.229	0.768	21.63	0.251	0.883	28.87	0.257
2DGS RGB	0.850	27.75	0.177	0.817	22.45	0.229	0.895	29.08	0.267
2DGS MeshSplats (our)	0.795	26.88	0.245	0.766	21.71	0.248	0.890	29.50	0.254

During the evaluation, three standard metrics are utilized: PSNR, SSIM (Wang et al., 2004), and LPIPS (Zhang et al., 2018).

Quantitative Results The performance of MeshSplats was evaluated across three benchmark datasets, as indicated above. The quantitative outcomes are summarized in Tab. 1. On the Mip-NeRF360 and Tanks and Temples datasets, results were observed to be comparable to existing methods, with SSIM, PSNR, and LPIPS metrics aligning closely with state-of-the-art approaches such as 3DGS (Kerbl et al., 2023) and RaySplats (Byrski et al., 2025). For instance, on the Mip-NeRF360 dataset, our method achieved scores comparable to rasterization-based techniques despite its mesh-based representation. Similarly, on the Tanks and Temples dataset, performance metrics remained competitive, reflecting robustness in outdoor scene reconstruction. It is noteworthy that MeshSplats exhibited superior performance on the Deep Blending dataset. This outcome suggests that our method is effective in managing intricate indoor geometries and transparency effects, as it surpasses several baseline methods and approaches the performance metrics of leading models such as 3DGS.

Qualitative Results It was observed that MeshSplats renders generated using Nvdiffrast exhibited a visual quality nearly identical to that of 3DGS without spherical harmonics, as illustrated in Fig. 5. Both methods demonstrated similar limitations in modeling reflections on transparent surfaces, such as glass, where approximations of light interactions led to artifacts. Slight reductions in detail were detected in high-frequency regions, such as dense grass, where MeshSplats supplied marginally coarser reconstructions. Notwithstanding these minor discrepancies, the overall fidelity of the outcomes of our model was found to be comparable to those produced by 3DGS, thereby underscoring its ability to replicate the strengths of Gaussian-based

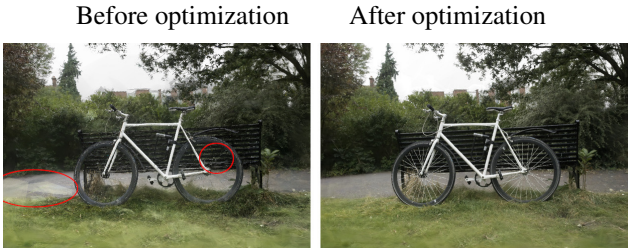


Figure 7. Comparison of the same scene before (left) and after (right) optimization rendered with Nvdiffrast. The unoptimized MeshSplats rendering is characterized by a lack of fine structural details, marked by red ellipses, such as missing or poorly defined bicycle spokes. Large floaters are observed in the scene, which detract from the overall coherence. In contrast, the optimized MeshSplats outcome shows significant refinement, with the floaters completely removed and finer details, including the spokes or grass, clearly reconstructed. It also exhibits improved geometric accuracy and visual clarity, with smoother surfaces and a more textured representation of the bike frame and surrounding elements.

rendering within a mesh-based framework.

Furthermore, when rendered using Blender’s EEVEE engine, MeshSplats also produced visually plausible results comparable to 3DGS, as shown in Fig. 6. However, challenges persisted in areas requiring intricate geometric precision, such as the fine leaf structures of the ficus scene, where high-frequency details were partially lost. Nevertheless, the majority of scenes retained photorealistic quality, with coherent geometry and accurate color representation. Minor artifacts, attributable to the mesh-based approximation of Gaussian opacity falloff, were observed but did not significantly detract from the overall visual integrity. These results affirm the adaptability of our method to traditional rendering pipelines while maintaining competitive rendering quality.

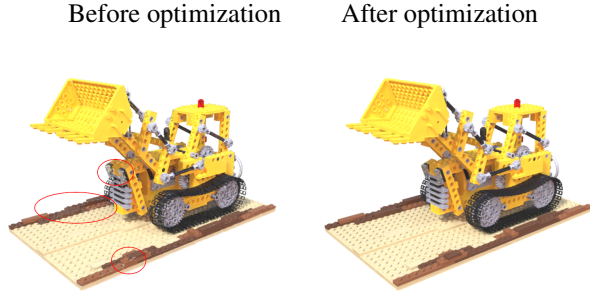


Figure 8. Comparison of the same scene before (left) and after (right) optimization, rendered in Blender using the EEVEE renderer. While our unoptimized model demonstrates potential, it exhibits a deficiency in detail, particularly along the edges of the excavator’s platform, as indicated by the red ellipses. It is noteworthy that the optimized MeshSplats (our) rendering does not manifest these issues.

Ablation Study MeshSplats can be used with a classical Gaussian Splatting, but it is dedicated to model scenes with flat Gaussians. Therefore, an ablation study was performed to compare our approach with three GS initialization variants: 3DGS (Kerbl et al., 2023), 2DGS (Huang et al., 2024), and GaMeS (Waczyńska et al., 2024). All methods were trained to generate splats using RGB color representations, omitting spherical harmonics to ensure compatibility with mesh rendering. Following training, the resulting Gaussian components were converted into unoptimized mesh soup. For flat Gaussians (2DGS and GaMeS), meshes were constructed by approximating each Gaussian as a polygon with eight triangles ($no_triag = 8$) and a scale multiplier of 2.7 ($scale_mul = 2.7$). For 3DGS, the transformation extended this process to three orthogonal surfaces, producing 3D mesh representations. Subsequently, MeshSplats was optimized using the Nvdiffrast renderer, which facilitated differentiable rasterization and blending with depth peeling. The optimization pipeline employed a combined L_1 and SSIM loss function, with vertex positions and colors updated iteratively over 15 epochs.

The results of the ablation study are presented in Tab. 2. When initialized with 3DGS, moderate performance degradation was observed on all datasets, due to the inherent complexity of fitting 3D Gaussians to mesh structures. For GaMeS, performance remained comparable to its RGB counterpart on Mip-NeRF360 and Deep Blending, indicating effective preservation of geometric fidelity despite the conversion. On the other hand, when initialized with 2DGS, MeshSplats achieved superior PSNR on Deep Blending with reduced LPIPS, demonstrating improved reconstruction quality in complex indoor scenes. While slight degradations were observed in outdoor datasets, the results

underscore the ability of our model to match or exceed its initialization methods in scenarios requiring fine-grained detail handling, despite its distinct mesh-based paradigm.

In addition, the impact of the optimization process on MeshSplats was thoroughly evaluated. As demonstrated in Fig. 7, the unoptimized model exhibited substantial floating objects (i.e., extraneous geometric artifacts) dispersed throughout the scene. Furthermore, high-frequency details, such as bicycle spokes and dense grass, were inadequately resolved or completely absent, leading to a diminution of geometric precision. During the optimization process, these limitations were addressed to a considerable extent. Specifically, floaters were removed, and fine structural elements, such as spokes and grass blades, were reconstructed with enhanced clarity. Similarly, in Fig. 8, challenges in sharp edge preservation for unoptimized meshes, marked with red ellipses, were also highlighted. Following the optimization process, there was a notable enhancement in edge sharpness and geometric coherence, resulting in more accurate rendition of complex geometries.

In summary, the results of the ablation study highlighted the importance of the optimization pipeline in enhancing the initial mesh conversion process. While unoptimized MeshSplats provided a reasonable starting point, the post-optimization phase was essential for reducing artifacts, improving detail retention, and reaching parity with cutting-edge rendering techniques.

5. Conclusions

In this paper, we introduce MeshSplats, a method that effectively overcomes the drawbacks of Gaussian Splatting (GS) by transforming it into a mesh-like structure, permitting its integration with ray tracing techniques. This adaptation enhances rendering quality by utilizing ray tracing’s benefits, such as improved lighting, shadows, and reflections. Our approach offers an immediate, practical solution and promises further enhancement through the MeshSplats optimization algorithm. The findings from an extensive experimental study corroborate the efficacy and adaptability of our technique, validating its wide applicability across diverse datasets. Notably, MeshSplats, despite its distinct mesh-based representation, has exhibited the capacity to render photorealistic scenes, attaining visual quality that is comparable to (or even surpassing) that of Gaussian Splatting techniques. The elimination of floaters and the refinement of structural details post-optimization further underscore its aptitude to balance geometric accuracy with rendering fidelity. These qualities reinforce the potential of our approach as a robust alternative for high-quality rendering in computer graphics and image processing.

Limitations Two key limitations of our approach have been identified. First, artifacts—such as fragmented geometry and opacity inconsistencies—tend to occur when modeling expansive, low-texture regions (e.g., the solid-color skies in the Train scene from the Tanks and Temples dataset). This issue arises from the mesh-based opacity interpolation, which struggles to reproduce the smooth fall-off characteristic of Gaussian elements in uniform areas. It is noteworthy that this problem did not manifest in DeepBlending’s indoor scenes featuring walls. Second, initialization with 3DGS produces densely tessellated meshes that lead to high vertex counts, thereby increasing memory usage and reducing rendering efficiency. Although the use of flat Gaussians (e.g., 2DGS, GaMeS) alleviates this issue, 3DGS-derived meshes remain computationally demanding for real-time applications.

References

- Barron, J. T., Mildenhall, B., Tancik, M., Hedman, P., Martin-Brualla, R., and Srinivasan, P. P. Mip-nerf: A multiscale representation for anti-aliasing neural radiance fields. In *Proceedings of the IEEE/CVF international conference on computer vision*, pp. 5855–5864, 2021.
- Barron, J. T., Mildenhall, B., Verbin, D., Srinivasan, P. P., and Hedman, P. Mip-nerf 360: Unbounded anti-aliased neural radiance fields. In *Proceedings of the IEEE/CVF conference on computer vision and pattern recognition*, pp. 5470–5479, 2022.
- Barron, J. T., Mildenhall, B., Verbin, D., Srinivasan, P. P., and Hedman, P. Zip-nerf: Anti-aliased grid-based neural radiance fields. In *Proceedings of the IEEE/CVF International Conference on Computer Vision*, pp. 19697–19705, 2023.
- Byrski, K., Mazur, M., Tabor, J., Dziarmaga, T., Kadziolka, M., Baran, D., and Spurek, P. Raysplats: Ray tracing based gaussian splatting. *arXiv preprint arXiv:2501.19196*, 2025.
- Chen, A., Xu, Z., Geiger, A., Yu, J., and Su, H. Tensorf: Tensorial radiance fields. In *European conference on computer vision*, pp. 333–350. Springer, 2022.
- Foley, J. D., Van Dam, A., Feder, S. K., Hughes, J. F., and Phillips, R. L. *Introduction to computer graphics*, volume 55. Addison-Wesley Reading, 1994.
- Fridovich-Keil, S., Yu, A., Tancik, M., Chen, Q., Recht, B., and Kanazawa, A. Plenoxels: Radiance fields without neural networks. In *CVPR*, pp. 5501–5510, 2022.
- Govindarajan, S., Rebain, D., Yi, K. M., and Tagliasacchi, A. Radiant foam: Real-time differentiable ray tracing. *arXiv preprint arXiv:2502.01157*, 2025.
- Gu, C., Wei, X., Zeng, Z., Yao, Y., and Zhang, L. Irgs: Inter-reflective gaussian splatting with 2d gaussian ray tracing. *arXiv preprint arXiv:2412.15867*, 2024.
- Guédon, A. and Lepetit, V. Sugar: Surface-aligned gaussian splatting for efficient 3d mesh reconstruction and high-quality mesh rendering. *CVPR*, 2024.
- Hedman, P., Philip, J., Price, T., Frahm, J.-M., Drettakis, G., and Brostow, G. Deep blending for free-viewpoint image-based rendering. *ACM Transactions on Graphics (ToG)*, 37(6):1–15, 2018.
- Huang, B., Yu, Z., Chen, A., Geiger, A., and Gao, S. 2d gaussian splatting for geometrically accurate radiance fields. In *ACM SIGGRAPH 2024 conference papers*, pp. 1–11, 2024.
- Jiang, Y., Tu, J., Liu, Y., Gao, X., Long, X., Wang, W., and Ma, Y. Gaussianshader: 3d gaussian splatting with shading functions for reflective surfaces. In *Proceedings of the IEEE/CVF Conference on Computer Vision and Pattern Recognition*, pp. 5322–5332, 2024.
- Kerbl, B., Kopanas, G., Leimkühler, T., and Drettakis, G. 3d gaussian splatting for real-time radiance field rendering. *ACM Trans. Graph.*, 42(4):139–1, 2023.
- Knapitsch, A., Park, J., Zhou, Q.-Y., and Koltun, V. Tanks and temples: Benchmarking large-scale scene reconstruction. *ACM Transactions on Graphics (ToG)*, 36(4):1–13, 2017.
- Ma, L., Agrawal, V., Turki, H., Kim, C., Gao, C., Sander, P., Zollhöfer, M., and Richardt, C. Specnerf: Gaussian directional encoding for specular reflections. In *Proceedings of the IEEE/CVF Conference on Computer Vision and Pattern Recognition*, pp. 21188–21198, 2024.
- Mildenhall, B., Srinivasan, P. P., Tancik, M., Barron, J. T., Ramamoorthi, R., and Ng, R. Nerf: Representing scenes as neural radiance fields for view synthesis. *Communications of the ACM*, 65(1):99–106, 2021.
- Moenne-Loccoz, N., Mirzaei, A., Perel, O., de Lutio, R., Martinez Esturo, J., State, G., Fidler, S., Sharp, N., and Gojcic, Z. 3d gaussian ray tracing: Fast tracing of particle scenes. *ACM Transactions on Graphics (TOG)*, 43(6):1–19, 2024.
- Müller, T., Evans, A., Schied, C., and Keller, A. Instant neural graphics primitives with a multiresolution hash encoding. *ACM Transactions on Graphics (ToG)*, 41(4):1–15, 2022.
- Munkberg, J., Hasselgren, J., Shen, T., Gao, J., Chen, W., Evans, A., Müller, T., and Fidler, S. Extracting triangular 3d models, materials, and lighting from images. In

-
- Proceedings of the IEEE/CVF Conference on Computer Vision and Pattern Recognition*, pp. 8280–8290, 2022.
- Parker, S. G., Bigler, J., Dietrich, A., Friedrich, H., Hoberock, J., Luebke, D., McAllister, D., McGuire, M., Morley, K., Robison, A., et al. Optix: a general purpose ray tracing engine. *Acm transactions on graphics (tog)*, 29(4):1–13, 2010.
- Peddie, J. *Ray Tracing: A Tool for All*. Springer Publishing Company, Incorporated, 1st edition, 2019. ISBN 3030174891.
- Tang, Z. J. and Cham, T.-J. 3igs: Factorised tensorial illumination for 3d gaussian splatting. Linprim: Linear primi In *European Conference on Computer Vision*, pp. 143–159. Springer, 2025.
- Verbin, D., Hedman, P., Mildenhall, B., Zickler, T., Barron, J. T., and Srinivasan, P. P. Ref-nerf: Structured view-dependent appearance for neural radiance fields. In *2022 IEEE/CVF Conference on Computer Vision and Pattern Recognition (CVPR)*, pp. 5481–5490. IEEE, 2022.
- Verbin, D., Srinivasan, P. P., Hedman, P., Mildenhall, B., Attal, B., Szeliski, R., and Barron, J. T. Nerf-casting: Improved view-dependent appearance with consistent reflections. In *SIGGRAPH Asia 2024 Conference Papers*, pp. 1–10, 2024.
- von Lützw, N. and Nießner, M. tives for differentiable volumetric rendering. *arXiv preprint arXiv:2501.16312*, 2025.
- Waczyńska, J., Borycki, P., Tadeja, S., Tabor, J., and Spurek, P. Games: Mesh-based adapting and modification of gaussian splatting. *arXiv preprint arXiv:2402.01459*, 2024.
- Wang, Z., Bovik, A. C., Sheikh, H. R., and Simoncelli, E. P. Image quality assessment: from error visibility to structural similarity. *IEEE transactions on image processing*, 13(4):600–612, 2004.
- Weyrich, T., Heinzle, S., Aila, T., Fasnacht, D. B., Oetiker, S., Botsch, M., Flaig, C., Mall, S., Rohrer, K., Felber, N., et al. A hardware architecture for surface splatting. *ACM Transactions on Graphics (TOG)*, 26(3):90–es, 2007.
- Xie, T., Chen, X., Xu, Z., Xie, Y., Jin, Y., Shen, Y., Peng, S., Bao, H., and Zhou, X. Envgs: Modeling view-dependent appearance with environment gaussian. *arXiv preprint arXiv:2412.15215*, 2024.
- Ye, K., Hou, Q., and Zhou, K. 3d gaussian splatting with deferred reflection. In *ACM SIGGRAPH 2024 Conference Papers*, pp. 1–10, 2024.
- Yu, Z., Chen, A., Huang, B., Sattler, T., and Geiger, A. Mip-splatting: Alias-free 3d gaussian splatting. In *Proceedings of the IEEE/CVF Conference on Computer Vision and Pattern Recognition*, pp. 19447–19456, 2024.
- Zhang, R., Isola, P., Efros, A. A., Shechtman, E., and Wang, O. The unreasonable effectiveness of deep features as a perceptual metric. In *Proceedings of the IEEE conference on computer vision and pattern recognition*, pp. 586–595, 2018.